At-wavelength characterization of the extreme ultraviolet Engineering Test Stand Set-2 optic

Patrick Naulleau,[a] Kenneth A. Goldberg, Erik H. Anderson, Phillip Batson, Paul E. Denham, Keith H. Jackson, Eric M. Gullikson, Senajith Rekawa, and Jeffrey Bokor[b]
Center for X-Ray Optics, Lawrence Berkeley National Laboratory, Berkeley, California 94720

(Received 11 June 2001; accepted 8 October 2001)

At-wavelength interferometric characterization of a new 4×-reduction lithographic-quality extreme ultraviolet (EUV) optical system is described. This state-of-the-art projection optic was fabricated for installation in the EUV lithography Engineering Test Stand (ETS) and is referred to as the ETS Set-2 optic. EUV characterization of the Set-2 optic is performed using the EUV phase-shifting point diffraction interferometer (PS/PDI) installed on an undulator beamline at Lawrence Berkeley National Laboratory's Advanced Light Source. This is the same interferometer previously used for the at-wavelength characterization and alignment of the ETS Set-1 optic. In addition to the PS/PDI-based full-field wave front characterization, we also present wave front measurements performed with lateral shearing interferometry, the chromatic dependence of the wave front error, and the system-level pupil-dependent spectral-bandpass characteristics of the optic; the latter two properties are only measurable using at-wavelength interferometry. © *2001 American Vacuum Society.* [DOI: 10.1116/1.1421545]

I. INTRODUCTION

The recent interest in extreme ultraviolet (EUV) lithography[1] has led to the development of a variety of novel metrologies. Because EUV optical systems utilize resonant-stack, reflective multilayer-coated optics,[2] performing metrology at the operational wavelength is essential to the development process.[3] This has led to numerous advancements in the field of EUV interferometry.[4–10] With a demonstrated reference-wave front accuracy of better than $\lambda_{EUV}/350$ (0.04 nm at $\lambda_{EUV} = 13.4$ nm),[10] the phase-shifting point diffraction interferometer (PS/PDI)[6,7] is, to the best of our knowledge, the highest accuracy EUV interferometer available.

Operating at the Advanced Light Source (ALS) synchrotron radiation facility at Lawrence Berkeley National Laboratory (LBNL), the PS/PDI has been in use for several years in the measurement and alignment of numerous small-field EUV 10×-reduction Schwarzschild objectives.[11] Independent verification of the accuracy of the PS/PDI and its utility in predicting and optimizing imaging performance has come from ongoing lithographic exposure experiments conducted at Sandia National Laboratories.[12]

More recently, a new interferometry endstation was constructed[8] specifically for at-wavelength testing of projection optics designed for the EUV-lithography engineering test stand (ETS).[13] This interferometer was used last year to characterize and align[8] the first of two projection optical systems[14] (the ETS Set-1 optic) which is currently installed in the operational ETS. Since that time, a second projection optic of higher quality (the ETS Set-2 optic) has been fabricated and assembled. The projection optics are four-mirror, aspheric ring-field systems, designed to operate at approximately 13.4 nm wavelength with a numerical aperture (NA) of 0.1 and 4× demagnification.

Here, we describe the characterization of the ETS Set-2 optic using at-wavelength interferometry. Installed on an undulator beamline, the PS/PDI (Fig. 1) is a versatile metrology tool, which can be configured to perform a variety of system-level interferometric and noninterferometric measurements. The interferometer is readily configurable as a lateral shearing interferometer[9] providing a significant increase in aberration magnitude measurement range, which is useful for initial system alignment. We present the use of the PS/PDI for the full-field wave front characterization of the ETS Set-2 optic. In addition to field-dependent wave front measurements, we also present the chromatic dependence of the wave front error, and the system-level pupil-dependent spectral-bandpass characteristics of the optic, properties that are only measurable at-wavelength.

II. PS/PDI CONFIGURATION

The PS/PDI was constructed to evaluate the system wave front at arbitrary positions across the field of view. In the object plane, the ring field is arc shaped, spanning 104 mm by 6 mm wide, and subtending 29°. Measurements of the field-dependent optical performance, across the large ring-field, provide feedback for the alignment of the individual mirror elements, enabling optimal imaging quality to be achieved.

The PS/PDI design (Fig. 1) has only a few critical optical components. All of the components exist in a vacuum environment with a base pressure of 10^{-7} Torr; a partial pressure of 10^{-5} Torr of oxygen gas is introduced as a pre-emptive contamination mitigation measure. Great care is taken to fol-

[a]Author to whom all correspondence should be addressed at LBNL, MS2-400, 1 Cyclotron Rd., Berkeley, CA 94720; electronic mail: pnaulleau@lbl.gov
[b]Also at: EECS Department, University of California, Berkeley, CA 94720.

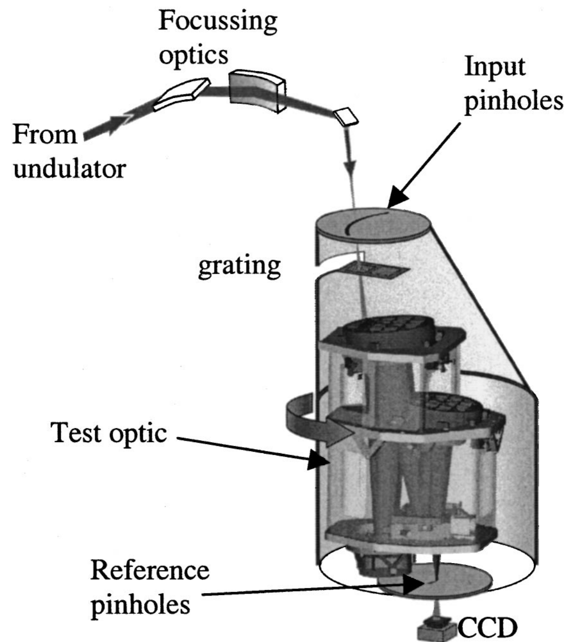

FIG. 1. Schematic of the EUV PS/PDI installed at an undulator beamline at LBNL ALS synchrotron radiation facility. A Kirkpatrick–Baez glancing-incidence optical system focuses the beamline radiation into a nominally 5 μm spot in the test optic object plane. Pinhole diffraction is used to produce both the probe and reference waves and a transmission grating is used as the beamsplitter.

low clean, UHV practices, and to ensure that only UHV compatible materials are introduced into the vacuum chamber. Once the interferometer component alignments were complete, an insulated thermal enclosure was constructed to contain the interferometer endstation and maintain temperature stability of 0.01 °C over 8 h.

Within the vacuum chamber, a synchrotron beam from an undulator source is focused onto the object (reticle) plane of the test optic from above; the illumination angle and position matches the design conditions. A Kirkpatrick–Baez glancing-incidence optical system focuses the beamline radiation into a fixed spot nominally 5 μm wide.

In the object (reticle) plane, diffraction from a small pinhole (the *object pinhole*) produces spatially coherent, spherical-wave illumination of the test optic, filling the pupil of the optical system with a divergence angle significantly larger than the input numerical aperture (NA) of the system. The size and quality of the spatial filtering pinhole play important roles in determining the spherical accuracy of the probe (test) beam.[7,10] A grating beamsplitter placed between the object pinhole and the test optic creates a series of overlapping coherent beams that are focused to laterally displaced positions in the image (wafer) plane. The image-plane beam separation is designed to be 5 μm. By propagating through the optical system, each of these overlapping beams acquires the characteristic aberrations of the test optic. In the image-plane, a patterned opaque and transparent (open stencil) mask selects two adjacent beams with all other beams being blocked. One of the two beams, the test beam, passes through a relatively large window in the mask, thereby preserving the aberrations imparted by the optical system. The second unblocked beam is focused onto a pinhole (the reference pinhole) smaller than the diffraction-limited resolution of the test optic, thereby producing an ideally spherical reference beam. The two beams propagate to the charge coupled device (CCD) where they overlap creating an interference pattern that records the deviation of the test beam from an ideal sphere.

To enable characterization of the test optic across the large field of view, the extended field is divided into 45 discrete field points, prescribed by the alignment method. The object and image-plane masks are comprised of arrays of pinholes and alignment features arranged to coincide with each field point position. The entire interferometer, including the test optic and the pinhole arrays, is moved under the stationary undulator beam, allowing the field points to be measured sequentially.

The pinhole arrays are fabricated with electron-beam lithography and reactive ion etching at LBNL's Nanowriter facility.[15] The masks are made up of a 200-nm-thick nickel absorbing layer evaporated onto 100-nm-thick low-stress silicon-nitride (Si_3N_4) membranes. The mask features are etched completely through the membrane prior to the Ni evaporation. Thus, the pinholes and windows are completely open in the finished masks, which maximizes their transmission and significantly mitigates contamination problems.

III. MEASUREMENT RESULTS

Prior to EUV characterization at LBNL, the ETS Set-2 optic was assembled, characterized, and aligned using visible-light interferometry at Lawrence Livermore National Laboratory.[16] The alignment was performed using an alignment algorithm developed for both EUV and visible-light interferometry.[17] The system was then brought to LBNL for at-wavelength characterization and re-alignment if deemed necessary.

A. Wave front measurements

At LBNL, three complete sets of interferometric measurements were performed over a five-week time period. Two initial measurements were performed using the shearing configuration[9] as the system temperature was reduced from the ALS ambient temperature of 24.5 °C to the designed operating temperature, 21.0 °C. All three measurements where performed at the optic centroid wavelength of 13.35 nm.

The two shearing measurements were performed at 22.6 and 20.9 °C, respectively. Although not described here in detail, some minor wave front temperature dependence [$\sim\lambda$/100 root-mean-square (rms)] was observed. Following stabilization of the interferometer endstation temperature, the system was configured for PS/PDI measurements and the entire field was again characterized. As described below, good agreement was found between the shearing and PS/PDI measurements.

Good qualitative agreement has also found between the first visible-light measurements and PS/PDI measurements described here. A more rigorous quantitative comparison is

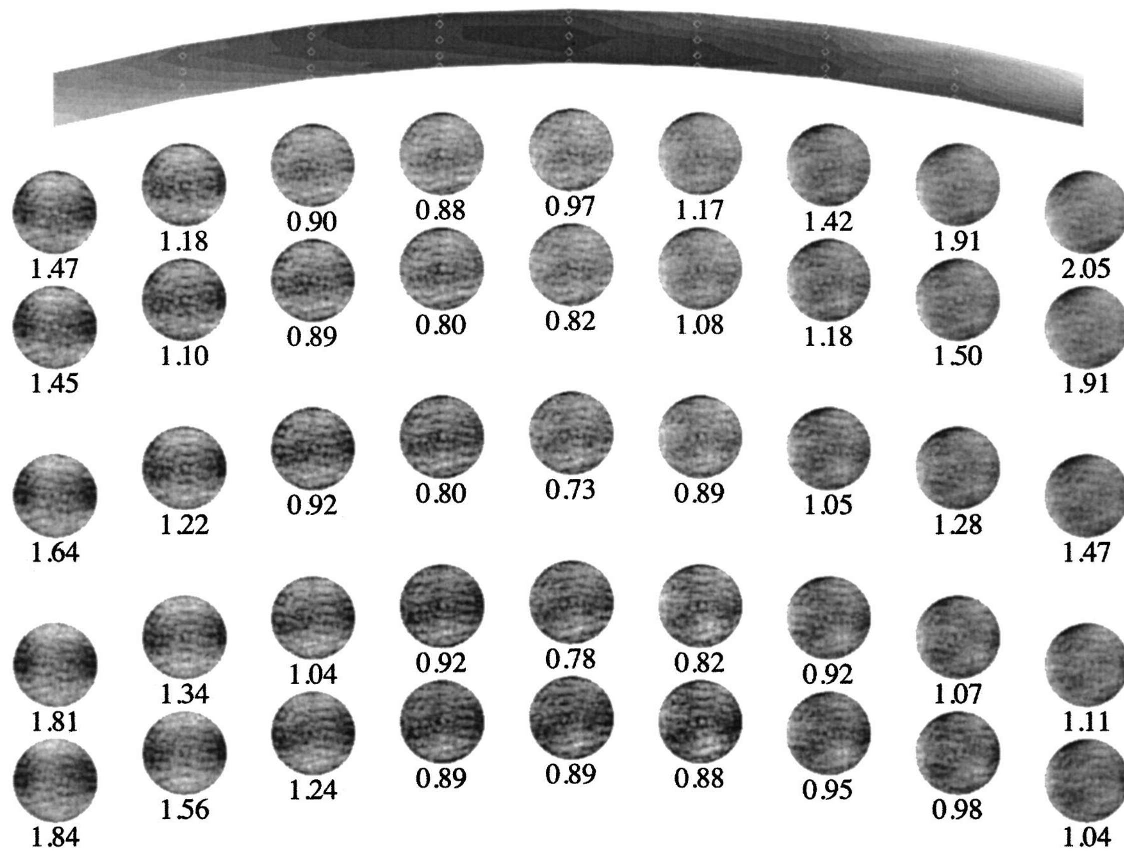

FIG. 2. Wave fronts measured at each of the 45 different field points and contour map of the rms error across the field. The gray-level steps in the contour map correspond to 0.1 nm increments. For display purposes, each wave front image is individually scaled to its own minimum and maximum values allowing detail to be seen in each wave front. The rms wavefront errors listed below each wave front are in nm and are based on a 37-term Zernike polynomial fit to the wave front with the measurement-dependent piston, tilt, and focus terms removed. The depicted wave fronts include higher spatial frequency content than is contained within the 37-term Zernike polynomial reconstructions.

now underway and will ultimately include a second set of visible-light measurements yet to be performed. The EUV measurements revealed that the system alignment had not changed appreciably during transport, temperature adjustment, and during the five weeks between the visible-light and EUV measurements. Due to the fact that good qualitative agreement was found, no subsequent alignment was performed based on the EUV measurements.

We note that quantitative comparisons performed with the ETS Set-1 optic[8] also showed very good wave front agreement, particularly for the midspatial-frequency wave front features. The EUV measurements were used to identify and correct systematic errors in the visible-light measurements, substantially improving the overall level of agreement. This level reached rms wave front difference magnitudes (rms magnitude of the point-by-point wave front difference) on the order of 0.25 nm, dominated by low-spatial-frequency wave front components, such as astigmatism.

Figure 2 shows wave front-characterization results determined from the final PS/PDI measurement. Figure 2 shows the individual wave fronts measured at each of the 45 different field points as well as a contour map of the rms error across the field. The rms wave front errors listed below each wave front are in nm and are based on a 37-term Zernike polynomial fit to the wave front[18] with the measurement-dependent piston, tilt, and focus terms removed. The depicted wave fronts include higher spatial frequency content than is contained within the 37-term Zernike polynomial reconstructions. At the best field point, a significant improvement in wave front quality (a factor of approximately 1.36) has been found relative to the Set-1 optic which had a rms wave front error ranging from 0.99 to 1.37 nm across the field of view.[8] Final analysis of the interferogram data is now underway. The final analysis will incorporate the results of interferometric null tests[10] that were performed to experimentally quantify the geometric systematic error magnitudes in the measurements. The final wave front error magnitudes are not expected to change by more than 0.02 nm from the values presented here.

Figure 3 shows the comparison between the final shearing measurement and the final PS/PDI measurement. The contour maps are based on the rms error over a NA of 0.0915 as limited by the measurement NA of the shearing implementation that was used.[9] The shearing measurement was performed using 2 μm pitch gratings placed approximately 300 μm from focus. For the comparison, the PS/PDI data was re-analyzed over the same 30×30 pixel grid size as used for the shearing. The coarser grid for shearing arises from the

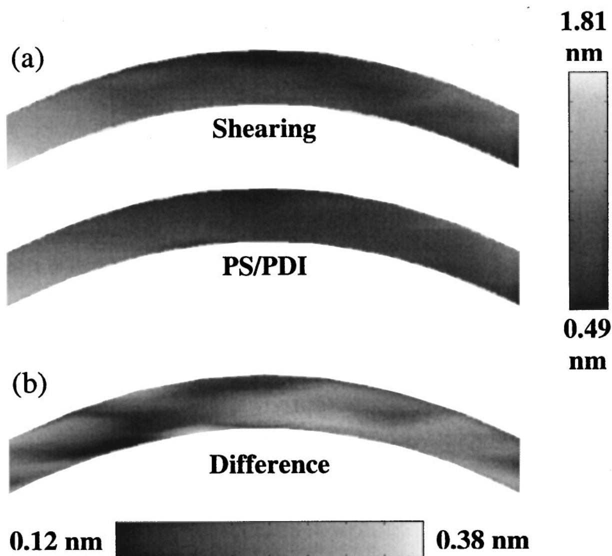

FIG. 3. Comparison between the final shearing measurement and the final PS/PDI measurement (both at wavelength). The contour maps are based on the rms error over a numerical aperture (NA) of 0.0915 as limited by the measurement NA of the shearing implementation used. For the comparison, the PS/PDI data was re-analyzed over the same grid size and NA as used for the shearing. The shearing and PS/PDI contour maps (a) are shown using a common colorscale. The contour map of the rms error of the difference wave fronts (b) is shown on a separate colorscale. The average agreement across the field is (0.25 ± 0.06) nm.

shear angle magnitude which is 1/15th of the NA angle. Between the shearing and PS/PDI, the average agreement across the field, as determined by the rms magnitude of the difference wave front, was found to be (0.25 ± 0.06) nm (λ/53) with the best agreement being 0.12 nm (λ/111). Based on separate characterization of the accuracy of the PS/PDI[10] and known limitations of the shearing implementation used here[9] (namely spurious interference terms from higher order grading diffraction terms), the agreement is expected to be limited by the accuracy of the shearing measurement.

B. Chromatic aberrations

One of the unique capabilities of the EUV interferometer is its ability to measure chromatic dependence of the wave front near the design operating wavelength.[19] In these measurements, a single field point is interferometrically probed as the illumination wavelength is tuned through a range exceeding the optic full-width-half-maximum spectral passband. Figure 4 shows the wave front change as a function of wavelength relative to the wave front measured at 13.35 nm wavelength. This measurement was performed at the central field point where the rms wave front error is approximately 0.73 nm. The difference-wave front precision, based on repeated measurements performed at a single wavelength, was measured at approximately 0.006 nm. The fact the wave front changes by less than $\lambda_{EUV}/500$ across a spectral band exceeding the 0.37 nm full-width-half maximum demonstrates the optic to be essentially free of chromatic aberrations.

C. Spectral bandpass

In addition to performing wave front measurements, the PS/PDI is also well suited to the characterization of system-level spectral-bandpass measurements. Moreover, because the optical system pupil is effectively projected onto the CCD, the spectral characteristics can be determined as a function of pupil position. In this case, the grating beamsplitter is removed from the system and pupil transmission images are recorded on the CCD as the wavelength is varied. Each CCD pixel is then treated as an independent detector from which the spectral response for the corresponding point in the pupil can be found.

Figure 5 shows the centroid wavelength change as a function of pupil position as measured at the central field point. The pupil map has been binned down to a 40-pixel grid. The average centroid wavelength is 13.35 nm with a peak-to-valley linear variation of (0.015 ± 0.002) nm across the pupil. The variation, which is oriented along the direction of large angles of incidence, is consistent with that expected from the optical design and the known coating parameters, which were measured after the coating of each individual mirror. Modeling results show an expected linear change of approximately 0.017 nm across the pupil.

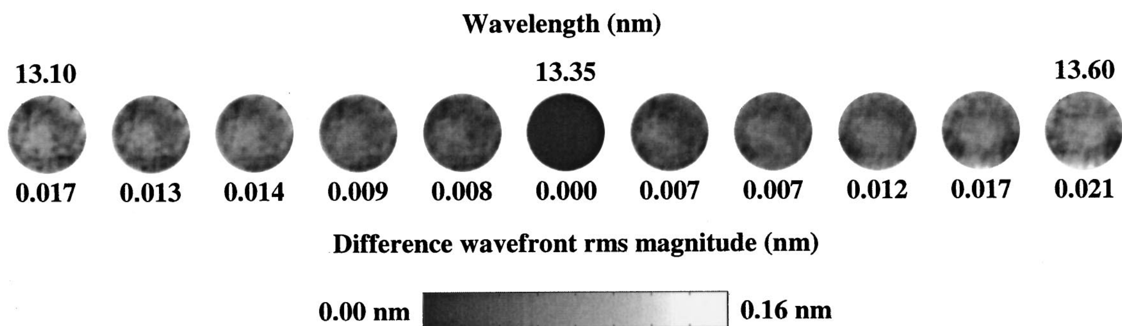

FIG. 4. Wave front variation, as a function of wavelength, relative to the wave front measured at a wavelength of 13.35 nm. This measurement was performed at the central field point where the wave front error is approximately 0.73 nm rms. The number below each wave front image is the rms magnitude of the difference wave front. The difference wave front images are all globally scaled as indicated by the colorbar.

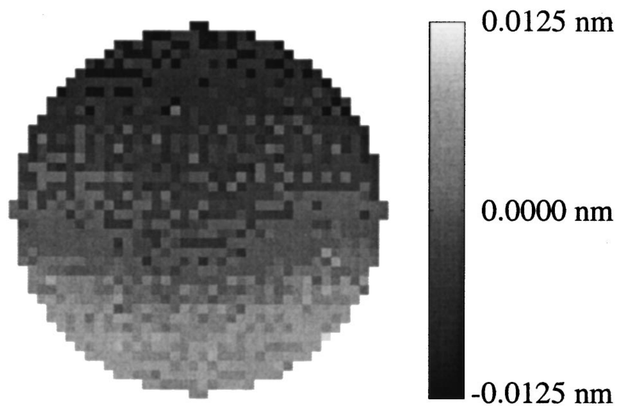

FIG. 5. Centroid wavelength change as a function of pupil position as measured at the central field point. The average centroid wavelength is 13.35 nm with a peak-to-valley linear variation of (0.015±0.002) nm across the pupil. Modeling results show an expected linear change of approximately 0.017 nm across the pupil.

IV. CONCLUSION

At-wavelength characterization of the ETS Set-2 optic has been completed and significant improvement over the Set-1 optic[8] was found. This characterization included both shearing and PS/PDI measurements across the field, chromatic aberration measurements, and pupil-position-dependent spectral-passband measurements. The spectral and chromatic measurements, which can only be performed at wavelength, demonstrated the extremely high quality of the EUV coatings. Having completed the at-wavelength characterization, the PS/PDI is now undergoing modifications that will allow it to be used to perform static printing experiments across the field.[20] These capabilities will allow the earliest possible imaging demonstration with the Set-2 optic before it is installed into the ETS for full-field scanned imaging.

ACKNOWLEDGMENTS

The authors are greatly indebted to Bruce Harteneck, Deirdre Olynick, and Eugene Veklerov for nanofabrication support, to Farhad Salmassi for coating support, to David Richardson and Ron Tackaberry for programming support, and to Brian Hoef, Drew Kemp, Gideon Jones, and Rene Delano for technical and fabrication support. This research was supported by the Extreme Ultraviolet Limited Liability Company and the DOE Office of Basic Energy Science.

[1]R. Stulen and D. Sweeney, IEEE J. Quantum Electron. **35**, 694 (1999).
[2]J. H. Underwood and T. W. Barbee, Jr., Appl. Opt. **20**, 3027 (1981).
[3]D. Attwood, G. Sommargren, R. Beguiristain, K. Nguyen, J. Bokor, N. Ceglio, K. Jackson, M. Koike, and J. Underwood, Appl. Opt. **32**, 7022 (1993).
[4]J. E. Bjorkholm, A. A. MacDowell, O. R. Wood II, Z. Tan, B. LaFontaine, and D. M. Tennant, J. Vac. Sci. Technol. B **13**, 2919 (1995).
[5]A. K. Ray-Chaudhuri, K. D. Krenz, and C. H. Fields, J. Vac. Sci. Technol. B **15**, 2462 (1997).
[6]H. Medecki, E. Tejnil, K. A. Goldberg, and J. Bokor, Opt. Lett. **21**, 1526 (1996).
[7]K. A. Goldberg, Ph.D. dissertation, University of California, Berkeley, 1997.
[8]K. A. Goldberg, P. Naulleau, P. Batson, P. Denham, E. Anderson, H. Chapman, and J. Bokor, J. Vac. Sci. Technol. B **18**, 2911 (2000).
[9]P. Naulleau, K. A. Goldberg, and J. Bokor, J. Vac. Sci. Technol. B **18**, 2939 (2000).
[10]P. Naulleau, K. Goldberg, S. Lee, C. Chang, D. Attwood, and J. Bokor, Appl. Opt. **38**, 7252 (1999).
[11]K. A. Goldberg, P. Naulleau, and J. Bokor, J. Vac. Sci. Technol. B **17**, 2982 (1999).
[12]G. F. Cardinale, C. C. Henderson, J. E. M. Goldsmith, P. J. S. Mangat, J. Cobb, and S. D. Hector, J. Vac. Sci. Technol. B **17**, 2970 (1999).
[13]D. Tichenor, A. Ray-Chaudhuri, W. Replogle, R. Stulen, G. Kubiak, P. Rockett, L. Klebanoff, K. Jefferson, A. Leung, J. Wronosky, L. Hale, H. Chapman, J. Taylor, J. Folta, C. Montcalm, R. Soufli, E. Spiller, K. Blaedel, G. Sommargren, D. Sweeney, P. Naulleau, K. Goldberg, E. Gullikson, J. Bokor, P. Batson, D. Attwood, K. Jackson, S. Hector, C. Gwyn, and P. Yan, Proc. SPIE **4343**, 19 (2001).
[14]D. W. Sweeney, R. Hudyma, H. N. Chapman, and D. Shafer, Proc. SPIE **3331**, 2 (1998).
[15]E. H. Anderson, V. Boegli, and L. P. Murray, J. Vac. Sci. Technol. B **13**, 2529 (1995).
[16]G. E. Sommargren, *Extreme Ultraviolet Lithography*, OSA Trends in Optics and Photonics Vol. 4, edited by G. D. Kubiak and D. R. Kania, (Optical Society of America, Washington, DC, 1996), pp. 108–112.
[17]H. N. Chapman and D. W. Sweeney, Proc. SPIE **3331**, 102 (1998).
[18]A. Bathia and E. Wolf, Proc. Phys. Soc. London, Sect. B **65**, 909 (1952).
[19]E. Tenjil, K. A. Goldberg, and J. Bokor, Appl. Opt. **37**, 8021 (1998).
[20]P. Naulleau, K. Goldberg, E. Anderson, P. Batson, P. Denham, S. Rekawa, and J. Bokor, Proc. SPIE **4343**, 639 (2001).